Published in final edited form as:

Dalton Trans. ; 51(33): 12540–12548. doi:10.1039/d2dt01852g.

Molybdenum (IV) Dithiocarboxylates as Single-Source Precursors for AACVD of MoS_2 Thin Films

Saleh Muhammad[a,b,‡], **Erik T. Ferenczy**[a,‡], **Ian M. Germaine**[a,‡], **J. Tyler Wagner**[a], **Muhammad T. Jan**[b], **Lisa McElwee-White**[a,†]

[a]Department of Chemistry, University of Florida, Gainesville, FL 32611-7200 USA

[b]Department of Chemistry, Islamia College Peshawar, 25120 Peshawar, Pakistan

Abstract

Tetrakis(dithiocarboxylato)molybdenum(IV) complexes of the type $Mo(S_2CR)_4$ (R = Me, Et, ^{i}Pr, Ph) were synthesized, characterized and prescreened as precursors for aerosol assisted chemical vapor deposition (AACVD) of MoS_2 thin films. The thermal behavior of the complexes as determined by TGA and GC-MS was appropriate for AACVD, although the complexes were not sufficiently volatile for conventional CVD bubbler systems. Thin films of MoS_2 were grown by AACVD at 500 °C from solutions of $Mo(S_2CMe)_4$ in toluene. The films were characterized by GIXRD diffraction patterns which correspond to a 2H-MoS_2 structure in the deposited film. Mo-S bonding in 2H-MoS_2 was further confirmed by XPS and EDS. The film morphology, vertically oriented structure and thickness (2.54 μm) were evaluated by FE-SEM. The Raman E^1_{2g} and A_{1g} vibrational modes of crystalline 2H-MoS_2 were observed. These results demonstrate the use of dithiocarboxylato ligands for the chemical vapor deposition of metal sulfides.

Graphical Abstarct

†Corresponding author: lmwhite@chem.ufl.edu.

‡S.M., E.T.F., and I.M.G. made equal contributions to this work.

Author Contributions

S.M., E.T.F., and I.M.G. carried out the precursor syntheses, materials growth, and film characterization. J.T.W. assisted with materials characterization. L.M.W. conceived and directed the research. All authors contributed to data analysis and writing of the manuscript.

Conflicts of interest

There are no conflicts to declare.

Electronic Supplementary Information (ESI) available: ^{1}H and $^{13}C\{^1H\}$ NMR spectra of all complexes, and ESI-HRMS for all complexes. See DOI: 10.1039/x0xx00000x

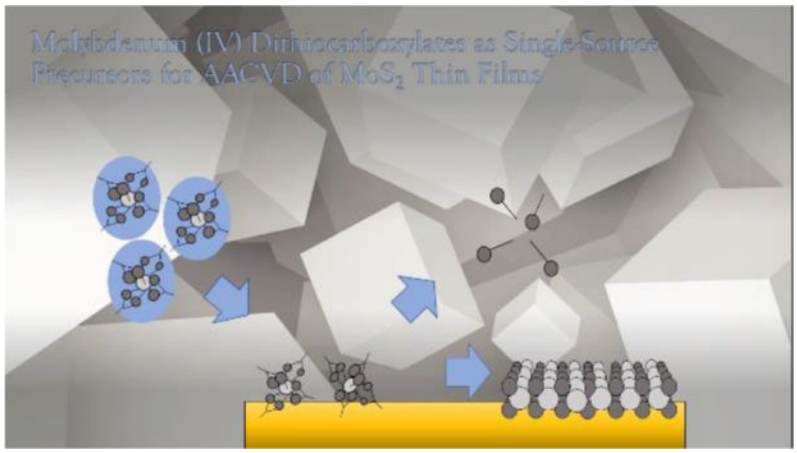

Deposition of MoS_2 from $Mo(S_2CMe)_4$ demonstrates use of dithiocarboxylate ligands for sulfur in single source precursors for TMD materials.

Introduction

Molybdenum disulfide (MoS_2) is a two-dimensional transition metal dichalcogenide with both metallic (1T, octahedral O_h) and semiconducting (2H, trigonal prismatic D_{3h}) polymorphs.[1] The semiconducting lattice has high electron mobility[2] and its indirect band gap in the bulk material[3, 4] increases to a direct band gap semiconductor as a monolayer.[5, 6] MoS_2 has found application in nanoelectronics,[7–10] optoelectronics,[11, 12] sensors,[13] batteries,[14–17] photovoltaics,[18] photodetectors,[19] phototransistors,[20] lubricants,[21–23] and catalysis.[11, 13, 24–26]

Because van der Waals forces hold the layers of MoS_2 together, physical exfoliation of bulk material[27–29] is possible for fundamental research and proof-of-concept devices. However, this is not practical for large scale application. Instead, a number of deposition methods are currently practiced. These include physical vapor deposition (PVD) processes such as sputtering[30, 31] and thermal evaporation.[32] Solution deposition methods have also been developed.[11, 33] Chemical vapor deposition (CVD)[13, 25, 34–36] and atomic layer deposition (ALD)[37] have also been used to deposit TMD materials with control over the stoichiometry and materials properties in the resultant film.[38] Development of CVD methods for TMD materials is of interest because CVD has the capacity to coat solid substrates with highly dense, pure films from gas phase precursors in large scale applications.[39, 40]

There are several coreactant systems in use for CVD of MoS_2. The most common coreactant pair is MoO_3 with sulfur.[20, 36, 41] It should be noted that methods that involve sulfiding MoO_3 films with elemental sulfur require high temperatures.[20, 41] Sulfur has also been reacted with $(NH_4)_6Mo_7O_{24}$ as the molybdenum source[42] and the reaction of K_2MoO_4 with sulfur has been used to prepare the 1T phase of MoS_2.[43] The N-bound ligand complexes $[Mo(N^tBu)_2(dpamd)_2]$ and $[Mo(N^tBu)_2(^tBu_2DAD)]$ have been used with sulfur as the coreactant for metal organic chemical vapor deposition, with minimal nitrogen content in the films.[44, 45] In CVD methods that use coreactant systems for the metal and the

chalcogen but do not use elemental sulfur, the sulfur content is often derived from toxic and hazardous precursors, such as H_2S,[46, 47] or diethyl sulfide.[48] These coreactant pairs include MoO_3/H_2S,[46] $MoCl_5/H_2S$,[47] $Mo(CO)_6/H_2S$,[49] $Mo(CO)_6/Et_2S$,[50] $Mo(CO)_6/CS_2$,[51] and Na_2MoO_4/Et_2S.[48]

An alternative approach is to deposit materials using a single-source precursor where a single compound contains all the elements found in the film.[52–55] The first reported single source precursor was the tetrakis(t-butylthiolato) complex $Mo(S^tBu)_4$, which could be used for growth of MoS_2 at low temperatures between 110 and 350 °C with minimal contamination of C from the ligands.[56] The molybdenum dithiocarbamate complex $Mo(Et_2NCS_2)_4$ has been used as a precursor for CVD of MoS_2 at 400 °C,[57] as well as for conversion to MoS_2 by pyrolysis[58] and air-spray deposition.[59, 60] The chelating dithiolate complex $Mo(SEtN(Me)EtS)_2$ was demonstrated to thermally decompose to MoS_2.[61] CVD of WS_2 from the tungsten analogue $W(SEtN(Me)EtS)_2$ provided evidence that the Mo complex would be suitable for CVD.

The challenges associated with the low volatility that is common in complexes of S-bound ligands that would otherwise be good single source precursor candidates[62] can be addressed by use of aerosol-assisted chemical vapor deposition (AACVD). In contrast to conventional CVD techniques where neat precursor is volatilized by evaporation or sublimation, AACVD is a variant where aerosolized droplets of precursor solutions transport the precursor with the assistance of a carrier gas.[40, 63] Thus, precursor candidates that have low volatility but reasonable solubility in appropriate solvents can be used in CVD. This approach has been demonstrated for deposition of MoS_2 by AACVD from the dithiocarbamate complexes $Mo(R_2NCS_2)_4$ (R = Et, ^{n}Bu) at 400–475 °C.[64] AACVD has been also been used to deposit Fe-doped MoS_2/Mo_2S_3 from $[CpMo(SMe)_2]_2$;[60] and the related technique mist CVD has been used to deposit MoS_2 from $(NH_4)_2MoS_4$.[65] We now report synthesis of a series of Mo(IV) dithiocarboxylate complexes of the type $Mo(S_2CR)_4$ as potential single source precursors and we demonstrate AACVD of MoS_2 from the methyl derivative $Mo(S_2CMe)_4$ (Figure 1).

Experimental Details

General Procedures

Synthetic reactions were carried out in Schlenk flasks or in a glove box under an N_2 atmosphere. All chemicals used were reagent grade and used without further purification unless noted. Methylmagnesium chloride (3.0 M in THF) and ethylmagnesium chloride (2.0 M in THF) were obtained from Sigma Aldrich (ACS grade, 99%+ purity). Isopropylmagnesium chloride (2.0 M in THF) was purchased from Acros Organics. Carbon disulphide (ACS grade, 99%+ purity) was obtained from Fisher. $MoCl_5$ and CH_3CN were obtained from Sigma Aldrich (ACS grade, 99%+ purity). Bromobenzene (99%) was purchased from Sigma Aldrich and was dried over activated 4 Å molecular sieves for over 24 h, then sparged with dry N_2 for five minutes. $MoCl_4(NCCH_3)_2$ was synthesized according to the literature.[66]

Solvents were air-free and dried using standard procedures: THF was distilled from sodium benzophenone ketyl and was stored over activated 4 Å molecular sieves. Carbon disulfide was distilled over CaH_2 under nitrogen. Acetonitrile was sparged with N_2 for 5 minutes and dried over activated 4 Å molecular sieves for at least 24 hours prior to use. Diethyl ether, Chloroform-*d* and benzene-d_6 (Cambridge Isotopes) were stored over 4 Å molecular sieves for 24 h prior to use. NMR spectra were recorded on Avance III HD 400 MHz and Avance III HD 600 MHz spectrometers and referenced to residual solvent peaks. Mass spectra were recorded on an Agilent 6230 Time-of-Flight instrument operating at 500 °C. The analysis was done in positive mode. The gas temperature was 350 °C, the drying gas was N_2 with a flow rate of 8.0 L/min. The pressure of the nebulizer was 30 psig. The sheath gas was N_2 with a temperature of 350 °C and a flow rate of 11.0 L/min. Elemental analyses were performed by Robertson Microlit Laboratories (Ledgewood, NJ).

Pyrolysis of $Mo(S_2CMe)_4$ was performed by loading a GC vial with 10 mg of sample inside a glove box under N_2, heating the vial to 250 °C for 45 min, then sampling the headspace with a gas-tight syringe. The GC-MS was performed on a ThermoScientific Trace GC Ultra gas chromatograph equipped with a Restek Corp. Rxi-5MS column. The MS transfer line and GC injection port were 250 °C. The injection mode was split with a flow rate of 10 mL/min. The temperature program was 35 °C (0–6 min) to 250 °C at 6 °C/min, then hold 3 min at 250 °C. The GC was coupled with a ThermoScientific DSQ II mass spectrometer using electron ionization at 70 eV. The ion source temperature was 250 °C. Detected peaks were identified using the NIST/EPA/NIH Mass Spectral Library, Version 2.3, build May 4, 2017.

Synthesis

Synthesis of $Mo(S_2CMe)_4$.—A 50 mL Schlenk flask equipped with a stir bar was flame dried, purged, and backfilled three times with dry nitrogen. Dry THF (25 mL) was added along with MeMgCl (3.0 M in THF, 4.2 mL, 13 mmol) via syringe. The flask was cooled in an ice water bath and dry CS_2 (0.85 mL, 14. mmol) was added dropwise via syringe. After addition the ice bath was removed, and the solution was allowed to stir under nitrogen overnight. The next day $MoCl_4(NCCH_3)_2$ (0.9864 g, 3.084 mmol) was weighed out in a glove box and added to the dithiocarboxylate solution under high N_2 flow. The mixture was initially brown then turned dark black after a few hours. It was stirred overnight at room temperature under nitrogen. The reaction mixture was filtered over a Celite pad on a medium porosity glass frit. Additional THF (100 mL) was used to wash the flask and the Celite pad. The filtrate was transferred to a clean flask and volatiles were removed under vacuum. The residue was then washed with 10 mL MeOH:H_2O (1:1) three times, followed by 10 mL of H_2O. The residue was isolated by filtration and was then dried under high vacuum for several hours. Crude yield: 1.1762 g (83%). Analytically pure product can be obtained by flash chromatography on silica using 1:1 DCM:hexanes as the mobile phase. Although the crystal structure of the compound is known,[67] no NMR data had been reported. ^{1}H NMR (400 MHz, C_6D_6): δ 2.04 (s, 12H, $Mo(S_2CCH_3)_4$). $^{13}C\{^1H\}$ NMR (101 MHz, C_6D_6): 38.9 ($Mo(S_2C\mathit{C}H_3)_4$), 228.9 ($Mo(S_2\mathit{C}CH_3)_4$). ESI-HRMS (methanol): *m/z* Calc. for $C_8H_{12}MoS_8$ [M^+]: 461.7759. Found: 461.7765. Elemental analysis: Calc. for $C_8H_{12}MoS_8$: C, 20.9; H, 2.6; S, 55.7; found: C, 21.1; H, 2.4; S, 56.3%.

Synthesis of $Mo(S_2CEt)_4$.—Synthesized in the same manner as $Mo(S_2CMe)_4$ using the following quantities of reagents: EtMgCl (2.0 M in THF, 6.3 mL, 13 mmol); THF (24 mL); CS_2(0.76 mL, 13 mmol); $MoCl_4(NCCH_3)_2$ (1.005 g, 3.142 mmol). The black residue obtained after aqueous workup was triturated with ca. 5 mL of methanol then dried under vacuum. Crude yield: 0.4476 g, 28%. Analytically pure sample can be obtained by flash chromatography on silica with gradient elution starting with pure hexanes and adding increasing amounts of THF. ^{1}H NMR (600 MHz, C_6D_6): δ 2.38 (q, 8H, SSCCH_2CH$_3$), 0.92 (t, 12H, SSCCH$_2$CH_3) ^{13}C{^{1}H} NMR (151 MHz, C_6D_6): δ 235.10 (Mo(S_2CCH_2CH$_3$)$_4$), 45.29 (Mo(S_2CCH_2CH$_3$)$_4$), 11.59 (Mo(S_2CCH$_2$CH_3)$_4$). IR (KBr) cm^{-1}: 2968 (m), 2920 (m), 2851 (m), 1452 (m), 1262 (m), 1169 (m), 1099 (s), 1045 (s), 1041 (s), 942 (m), 803 (m). ESI-HRMS (methanol): *m/z* Calc. for $C_{12}H_{20}MoS_8$ [M^+]: 517.8385. Found: 517.8371. Elemental analysis: Calc. for $C_{12}H_{20}MoS_8$: C, 27.9; H, 3.9; S, 49.6; found: C, 27.9; H, 3.7; S, 49.7%

Synthesis of $Mo(S_2C^iPr)_4$.—The compound was synthesized in the same manner as $Mo(S_2CMe)_4$ with the following quantities of reagents: THF (25 mL), ^{i}PrMgCl (2.0 M in THF, 6.3 mL, 13. mmol), CS_2 (0.85 mL, 14. mmol), $MoCl_4(NCCH_3)_2$ (1.0147 g, 3.1723 mmol). The filtrate was dried under vacuum and 10 mL of MeOH/H_2O (1:1) was added to the residue. The oily mixture was transferred to a separatory funnel, diluted with 10 mL DI water and rinsed with diethyl ether (50 mL x3). The ether layers were collected, dried with $MgSO_4$, filtered, and volatiles were removed under vacuum, yielding a black oily residue. Crude yield: 1.418 g (78%). ^{1}H NMR (600 MHz, C_6D_6): δ 2.56 (septet, 1H), 1.04 (d, 6H). ^{13}C{^{1}H} NMR (151 MHz, C_6D_6): δ 240.38 (Mo(S_2C$CH(CH_3)_2$)$_4$), 49.49 (Mo(S_2C$CH(CH_3)_2$)$_4$), 21.40 ppm (Mo(S_2CCH(CH_3)$_2$)$_4$). ESI-HRMS (methanol): *m/z* Calc. for $C_{16}H_{28}MoS_8$ [M^+]: 573.9011. Found: 573.8971.

Synthesis of $Mo(S_2CPh)_4$.—Phenylmagnesium bromide (2.0 M) was prepared using Mg turnings (0.4683 g, 19.27 mmol), dry THF (9.5 mL), and bromobenzene (2.0 mL, 19. mmol) with a catalytic iodine crystal. The compound was synthesized in the same manner as $Mo(S_2CMe)_4$ using the following quantities of reagents: dry THF (24 mL), PhMgBr (2.0 M in THF, 6.3 mL, 19. mmol), CS_2 (0.80 mL, 13. mmol), $MoCl_4(NCCH_3)_2$ (1.0269 g, 3.2105 mmol). The reaction mixture was filtered using a Celite pad on a medium porosity glass frit. Additional THF (100 mL) was used to wash the flask and the celite pad. The filtrate was transferred to a clean flask and volatiles were removed under vacuum. The residue was washed with 10 mL of MeOH/H_2O (1:1) three times followed by 10 mL of pentane three times, then the black solid was dried under vacuum. Crude yield: 2.1538 g (95%). Analytically pure sample was obtained by placing a saturated DCM solution into −20 °C freezer overnight, then decanting off the supernatant and drying the needle-like crystals for several hours under high vacuum. The compound was characterized by comparison to literature data.[68, 69] ^{1}H NMR (400 MHz, C_6D_6): δ 6.81 (d, 2H, meta), 6.94 (t, 1H, para), 7.81 (t, 2H, ortho). ^{13}C{^{1}H} NMR (101 MHz, C_6D_6): δ 216.77 (dithiocarboxylate), 141.40 (C_{para}), 132.84 (C_{ipso}), 128.40 (C_{meta}), 123.46 (C_{ortho}) ppm. Elemental analysis: Calc. for $C_{28}H_{20}MoS_8$: C, 47.4; H, 2.8; S, 36.1; found: C, 47.4; H, 2.5; S, 37.8%.

Aerosol Assisted Chemical Vapor Deposition (AACVD).—Depositions were performed using a commercial Blue Wave Semiconductor CVD reactor equipped with a Liquifog ultrasonic liquids atomizer (1.6 MHz) from Johnson Matthey Piezoproducts. The chamber was cleaned with acetone and evacuated to 5.20×10^{-2} Torr, 4 h prior to deposition. The substrates used were Si<100> with native oxides, which were cut into 1 cm^2 squares, then cleaned by boiling in acetone, methanol, and deionized water each for five minutes. Precursor solutions (0.017 M) were prepared in a nitrogen-filled glovebox using 40 mL of toluene. High-purity nitrogen (99.999% purity, 200 sccm) was used as a carrier gas, and the reactor pressure was maintained at 350 Torr with a deposition period of 110 min and a substrate temperature of 500 °C.

Materials Characterization—Thermogravimetric analysis (TGA) was performed on a TA Instruments TGA 5500 under N_2 flow, with a temperature increase from 25 to 650 °C at a heating rate of 20 °C /min. Field emission scanning electron microscopy (FE-SEM) and energy dispersive X-ray spectroscopy (EDS) were performed on an FEI Nova 430 instrument with an accelerating voltage of 3.5 keV. Grazing incidence X-Ray diffraction (GIXRD) was performed on a Panalytical X'Pert Materials Research Diffractometer (MDR) at a scanning rate of 1.2° min^{-1}, at the range of 25–65°30. X-ray photoelectron spectroscopy measurements were collected using an ULVAC Phi Versaprobe 4 XPS, working with a monochromatic aluminium anode (1486.6 eV) as the X-ray source. Raman spectra were measured on a Horiba microRaman instrument using a 532 nm excitation laser at 10X magnification.

Results and discussion

Synthesis of Precursors

The tetrakis (dithiocarboxylato) molybdenum complexes were synthesized by first generating the dithiocarboxylate ligand in situ[70] by reacting a Grignard reagent with carbon disulfide in THF and then adding $MoCl_4(NCCH_3)_2$, which is a readily available source of Mo(IV).[66, 71] The scheme can be seen in Figure 2. A similar method was used to synthesize tetrakis(dithiobenzoate) molybdenum complexes from $MoCl_4$(butyronitrile)$_2$ and various isolable dithiobenzoic acids in benzene.[68] The aliphatic dithiocarboxylate ligands used in this work were reported not to be isolable,[70] so we elected to generate them in situ. Purification of the complexes was achieved by column chromatography, liquid-liquid extraction, or recrystallization as noted in the experimental section. The isopropyl derivative $Mo(S_2C^iPr)_4$ was not successfully purified by these methods and remained a crude oil despite multiple attempts with various techniques. The complexes synthesized in this work are all dark coloured and appear to be bench stable for a period of months.

Spectroscopic Characterization of Precursors

All complexes synthesized were characterized using ^1H and ^{13}C NMR spectroscopy. The proton spectrum of $Mo(S_2CMe)_4$ showed a singlet at 2.04 ppm. The carbon spectrum showed two resonances, one at 38.9 ppm representing the methyl carbon, and one at 228.9 ppm representing the quaternary carbon. The proton spectrum of $Mo(S_2CEt)_4$ showed two resonances: a triplet at 0.92 ppm with an integration of 12H and a quartet at 2.38 ppm with

an integration of 8H. The carbon spectrum of $Mo(S_2CEt)_4$ showed three resonances at 11.59 ppm, 45.29 ppm, and 235.10 ppm. The proton spectrum of crude $Mo(S_2C^iPr)_4$ showed a doublet at 1.04 ppm and a septet at 2.56 ppm. The carbon spectrum of crude $Mo(S_2C^iPr)_4$ displayed three resonances at 21.40 ppm, 49.49 ppm, and 240.38 ppm. $Mo(S_2CPh)_4$ showed three resonances in the proton spectrum: a triplet at 6.81 ppm with an integration of 2H corresponding to the meta protons, a triplet at 6.94 ppm with an integration of 1H corresponding to the para proton, and a doublet at 7.81 ppm with an integration of 2H corresponding to the ortho protons. The carbon spectrum of $Mo(S_2CPh)_4$ showed five resonances: 123.46 ppm (C_{ortho}), 128.40 (C_{meta}), 132.84 (C_{ipso}), 141.39 (C_{para}), and 216.75 ppm (dithiocarboxylate).

Thermal Analysis of Precursors

The three complexes that could be obtained analytically pure were assessed for thermal properties via thermogravimetric analysis (TGA, Figure 3). $Mo(S_2CMe)_4$ had the lowest onset of decomposition temperature at around 90 °C with the initial and steepest mass loss at 170 °C followed by a second mass loss at 360 °C. The final residual mass was 51.3%. The calculated mass % for MoS_2 from $Mo(S_2CMe)_4$ would be 32.8%, indicating the decomposition of the precursor to MoS_2 is incomplete under these conditions. $Mo(S_2CEt)_4$ showed greatest mass loss around 152 °C followed by a series of other mass loss events around 210, 250 and 350 °C. The residual mass was 45.2% with a calculated residual mass for decomposition to MoS_2 of 30.9%. $Mo(S_2CPh)_4$ was the most thermally stable compound, not exhibiting any mass loss until a sharp mass loss event around 242 °C followed by a second major mass loss event around 325 °C. The ending residual mass was 33.3% as compared to a calculated residual mass of 22.6% for MoS_2. The stepped nature of the TGA curves and the large residual masses for all three complexes are consistent with incomplete thermal decomposition to MoS_2 in the bulk material. $Mo(S_2C^iPr)_4$ was not analysed via TGA because a pure sample could not be obtained. The decomposition evident in these TGA profiles indicates that these complexes are more appropriate for AACVD than for traditional CVD using direct volatilization in a bubbler.

Pyrolysis of the methyl derivative under nitrogen followed by sampling the headspace using GC-MS was done to identify thermal decomposition products. The primary fragments detected were hydrogen sulfide (46.5%) and carbon disulfide (16.6%). Methanethiol and ethanethiol were detected in trace amounts. Due to the ratio of molybdenum to sulfur being 1:8 in the complex and only 1:2 in the desired film, the evolution of sulfur-containing molecules is expected during growth of the film.

Mass Spectrometry of Precursors

Mass spectrometry can be used to provide insight into the decomposition behavior of CVD precursors, although some discretion must be used in interpreting the data as CVD is thermally-driven on a surface rather than the result of electron bombardment in the gas-phase.[72, 73] Direct Insertion Probe-Electron Ionization Mass Spectrometry (DIP-EI/MS) in positive ion mode was used to obtain electron impact fragmentation patterns for all four complexes. The mass spectrum of $Mo(S_2CMe)_4$ and possible structures of selected fragments can be seen in Figure 4. For all compounds analyzed, the base peak corresponded

to the thioacylium cation containing the corresponding R group (Table 1) This is consistent with a decomposition pathway involving the cleavage of a dithiocarboxylate ligand to generate a terminal sulfido ligand with loss of the thioacylium ion. Relevance of the mass spectra to the thermal decomposition pathways during deposition is demonstrated by comparison to the TGA curves in Fig. 3, which show that the residual mass for each compound after the initial mass loss (Me: 170 °C, Et: 152 °C, Ph: 242–276 °C) roughly corresponds to the loss of one thioacylium (RCS) fragment: Me: 87%, Et: 89%, and Ph: 83%. For $Mo(S_2C^iPr)_4$ and $Mo(S_2CPh)_4$, molybdenum-containing fragments can be observed which correspond to the loss of one or two thioacylium fragments. These fragments were not detected for $Mo(S_2CMe)_4$ and $Mo(S_2CEt)_4$. For $Mo(S_2CMe)_4$, $Mo(S_2CEt)_4$, and $Mo(S_2C^iPr)_4$, a molybdenum-containing fragment corresponding to the loss of one entire dithiocarboxylate ligand was detected. This was not detected for $Mo(S_2CPh)_4$.

Aerosol Assisted CVD of MoS_2.

Toluene solutions of $Mo(S_2CMe)_4$ (0.017 M, 40 mL) were used to deposit MoS_2 films by AACVD at a growth temperature of 500°C on Si ⟨100⟩ substrates with native oxide. After cooling down to 70 °C, the substrates had a silvery shiny appearance due to the deposited films. The deposited materials were characterized by FE-SEM, EDS, GIXRD, Raman spectroscopy, and XPS.

Materials Characterization

Field Emission Scanning Electron Microscopy (FE-SEM).

FE-SEM was performed on a film grown on $Si(100)/SiO_2$ at 500 °C via AACVD from $Mo(S_2CMe)_4$ in toluene (0.017 M) to assess the coverage, film morphology, and thickness of the film. Coverage of the substrate is complete and the vertically oriented platelike structure of the film parallels what has been observed with other bulk 2H-MoS_2 films deposited via CVD.[74–78] The film morphology grown at 500 °C in toluene does not match the tubular structure reported for films grown from $Mo[S_2CNR)_4]$, complexes grown from THF solutions at 400 and 425 °C but the differences can be attributed to changes in ligands, solvent, and temperature.[64] The thickness of the film was measured at approximately 2.54 μm from a cross-sectional image. Images of both the in-plane view and cross-sectional view can be seen in Figure 5. Another deposition trial using $Mo(S_2CMe)_4$ in toluene (40 mL, 0.017 M, 350 Torr, 200 sccm, N_2 carrier gas) at 600 °C resulted in a mixed morphology consisting of the vertically oriented structures as well as globular clusters. An FE-SEM image of this film can be seen in Fig. S-13 and its Raman spectrum appears in Fig. S-14.

Energy-dispersive X-ray spectroscopy (EDS).

EDS was performed to analyze the elemental composition of the film. An accelerating voltage of 5 keV was used. The S Kα and Mo Lα peaks overlap at around 2.3 keV, making it impossible to quantify the relative abundance of each element. The presence of carbon (Kα) and small amount of oxygen (Kα) can be observed at 0.28 keV and 0.53 keV, respectively. The EDS spectrum can be seen in Figure 6.

Grazing-Incidence X-ray Diffraction.

Grazing incidence X-ray diffraction (GIXRD) was used to investigate the crystal structure and crystallinity of the deposit grown from $Mo(S_2CMe)_4$ at 500 °C (Figure 7). The diffraction peaks were observed at 2θ = 33.26°, 38.96° and 58.76°, which correspond to (101), (103) and (110) planes of crystalline hexagonal 2H-MoS_2, respectively (JCPDS No. 37–1492).

Raman Spectroscopy.

Raman spectroscopy is a powerful tool to determine the presence of MoS_2 in a sample.[79] The film grown at 500 °C showed characteristic peaks at 373 cm^{-1} and 403 cm^{-1} that correspond to the E^1_{2g} and A_{1g} phonon modes of bulk MoS_2, respectively. An image of this spectrum can be seen in Figure 8.

X-ray Photoelectron Spectroscopy.

XPS was used to examine the chemical composition of the deposits for MoS_2 grown at 500 °C. A survey scan of the as-deposited MoS_2 revealed that Mo, S, C, O, and Si were present on the surface (Figure 9a). The sample was sputtered aggressively for several cycles of 3–4 min with 2000 eV Ar^+ ions to remove the oxidized surface layer and any surface bound intermediates. The survey spectrum after sputtering displayed reduced intensities of the C 1s and O 1s peaks, which indicated that carbon and oxygen present in the deposits were introduced postgrowth upon exposure to air. Due to the roughness of the deposited surface, not all of the C and O can be removed by sputtering and more aggressive sputtering dramatically changed the chemical composition of the material.

After the sample was sputtered under lighter conditions (250 eV), high resolution scans were obtained for the Mo 3d and S 2p regions (Figure 9b,c). The Mo 3d spectrum shows a Mo $3d_{5/2}$ and Mo $3d_{3/2}$ doublet at 229.6 and 232.6 eV, respectively, with an intensity ratio of 3:2 and a peak separation of 3.0 eV, corresponding to Mo^{4+} in MoS_2.[80] The peak at 226.5 was assigned to the S 2s BE of MoS_2. In the S 2p region, a doublet of S $2p_{3/2}$ and S $2p_{1/2}$ at 162.4 and 163.6 eV, respectively, was observed. The doublet had a separation of 1.2 eV with an intensity ratio of 2:1, and was assigned to S^{2-} in MoS_2.[80] No other species were observed in the high-resolution scans.

Conclusions

The homoleptic tetrakis(dithiocarboxylato)molybdenum(IV) complexes $Mo(S_2CMe)_4$, $Mo(S_2CEt)_4$, $Mo(S_2C^iPr)_4$, and $Mo(S_2CPh)_4$ were synthesized and characterized using ^1H and ^{13}C NMR. TGA revealed multi-step decomposition and volatilization processes for all complexes, making them more suitable as AACVD precursors than for use in conventional bubblers. DIP-EI/MS of all four complexes revealed a common base peak which corresponded to the thioacylium fragment $[SCR]^+$, where R = Me, Et, iPr, and Ph. Pyrolysis of $Mo(S_2CMe)_4$ and sampling of the headspace by GC/MS showed the decomposition products H_2S, CS_2, CH_3CH_2SH, and CH_3SH.

Aerosol-assisted chemical vapor deposition onto silicon substrates at 500 °C using toluene solutions of $Mo(S_2CMe)_4$ as a single source precursor yielded black matte films. The deposited material was identified as MoS_2 via Raman spectroscopy and GI-XRD. The films were further characterized using XPS, SEM, and EDS. These experiments demonstrate that dithiocarboxylate ligands can be used in as a sulfur source in CVD of transition metal dichalcogenide films.

Supplementary Material

Refer to Web version on PubMed Central for supplementary material.

Acknowledgements

SM acknowledges the Higher Education Commission (HEC), Pakistan for financial assistance. We thank the UF Mass Spectrometry Research and Education Center, supported by NIH S10 OD021758–01A1, for mass spectrometry data.

Notes and references

1. Lin Y-C, Dumcenco DO, Huang Y-S and Suenaga K, Nat. Nanotechnol, 2014, 9, 391. [PubMed: 24747841]
2. Radisavljevic B, Whitwick MB and Kis A, ACS Nano, 2011, 5, 9934–9938. [PubMed: 22073905]
3. Ryou J, Kim Y-S, Kc S and Cho K, Sci. Rep, 2016, 6, 29184. [PubMed: 27378032]
4. Gusakova J, Wang XL, Shiau LL, Krivosheeva A, Shaposhnikov V, Borisenko V, Gusakov V and Tay BK, Phys. Status Solidi A, 2017, 214, 1700218.
5. Splendiani A, Sun L, Zhang Y, Li T, Kim J, Chim C-Y, Galli G and Wang F, Nano Lett, 2010, 10, 1271–1275. [PubMed: 20229981]
6. Mak KF, Lee C, Hone J, Shan J and Heinz TF, Phys. Rev. Lett, 2010, 105, 136805. [PubMed: 21230799]
7. Butler SZ, Hollen SM, Cao L, Cui Y, Gupta JA, Gutiérrez HR, Heinz TF, Hong SS, Huang J, Ismach AF, Johnston-Halperin E, Kuno M, Plashnitsa VV, Robinson RD, Ruoff RS, Salahuddin S, Shan J, Shi L, Spencer MG, Terrones M, Windl W and Goldberger JE, ACS Nano, 2013, 7, 2898–2926. [PubMed: 23464873]
8. Podzorov V, Gershenson ME, Kloc C, Zeis R and Bucher E, Appl. Phys. Lett, 2004, 84, 3301–3303.
9. Radisavljevic B, Radenovic A, Brivio J, Giacometti V and Kis A, Nat. Nanotechnol, 2010, 6, 147–150.
10. Gong C, Zhang H, Wang W, Colombo L, Wallace RM and Cho K, Appl. Phys. Lett, 2013, 103, 053513.
11. Lv R, Robinson JA, Schaak RE, Sun D, Sun Y, Mallouk TE and Terrones M, Acc. Chem. Res, 2015, 48, 56–64. [PubMed: 25490673]
12. Chen Y, Xi J, Dumcenco DO, Liu Z, Suenaga K, Wang D, Shuai Z, Huang Y-S and Xie L, ACS Nano, 2013, 7, 4610–4616. [PubMed: 23600688]
13. Tan C and Zhang H, Chem. Soc. Rev, 2015, 44, 2713–2731. [PubMed: 25292209]
14. Zhou J, Qin J, Zhang X, Shi C, Liu E, Li J, Zhao N and He C, ACS Nano, 2015, 9, 3837–3848. [PubMed: 25791011]
15. Liu Q, Weijun X, Wu Z, Huo J, Liu D, Wang Q and Wang S, Nanotechnology, 2016, 27, 175402. [PubMed: 26965193]
16. Li XL, Li TC, Huang S, Zhang J, Pam ME and Yang HY, ChemSusChem, 2020, 13, 1379–1391. [PubMed: 31821700]
17. Chang K and Chen W, ACS Nano, 2011, 5, 4720–4728. [PubMed: 21574610]
18. Fontana M, Deppe T, Boyd AK, Rinzan M, Liu AY, Paranjape M and Barbara P, Sci. Rep, 2013, 3, 1634. [PubMed: 23567328]

19. Liu S, Nie C, Zhou D, Shen J and Feng S, Phys. E, 2020, 117, 113592.
20. Zhang W, Huang J-K, Chen C-H, Chang Y-H, Cheng Y-J and Li L-J, Adv. Mater, 2013, 25, 3456–3461. [PubMed: 23703933]
21. McCain MN, He B, Sanati J, Wang QJ and Marks TJ, Chem. Mater, 2008, 20, 5438–5443.
22. Cho D-H, Jung J, Kim C, Lee J, Oh S-D, Kim K-S and Lee C, Nanomaterials, 2019, 9, 293.
23. Fleischauer PD and Bauer R, Tribol. Trans, 1988, 31, 239–250.
24. Tummala P, Lamperti A, Alia M, Kozma E, Nobili LG and Molle A, Materials, 2020, 13, 2786.
25. Chhowalla M, Shin HS, Eda G, Li L-J, Loh KP and Zhang H, Nat. Chem, 2013, 5, 263–275. [PubMed: 23511414]
26. Alonso-Nunez G, Huirache-Acuna R, Paraguay-Delgado F, Lumbreras JA, Garcia-Alamilla R, Castillo-Mares A, Romero R, Somanathan R and Chianelli RR, Catal. Lett, 2009, 130, 318–326.
27. Li H, Wu J, Yin Z and Zhang H, Acc. Chem. Res, 2014, 47, 1067–1075. [PubMed: 24697842]
28. Ma R and Sasaki T, Acc. Chem. Res, 2015, 48, 136–143. [PubMed: 25490186]
29. Raza A, Hassan JZ, Ikram M, Ali S, Farooq U, Khan Q and Maqbool M, Adv. Mater. Interfaces, 2021, 8, 2002205.
30. Kaindl R, Bayer BC, Resel R, Muller T, Skakalova V, Habler G, Abart R, Cherevan AS, Eder D, Blatter M, Fischer F, Meyer JC, Polyushkin DK and Waldhauser W, Beilstein J. Nanotech, 2017, 8, 1115–1126.
31. Serpini E, Rota A, Ballestrazzi A, Marchetto D, Gualtieri E and Valeri S, Surf. Coat. Technol, 2017, 319, 345–352.
32. Sivarajan S and Padmanabhan R, Materials Today: Proceedings, 2016, 3, 2532–2536.
33. Hedlund JK and Walker AV, J. Chem. Phys, 2019, 150, 174701. [PubMed: 31067898]
34. Zhou D, Shu H, Hu C, Jiang L, Liang P and Chen X, Cryst. Growth Des, 2018, 18, 1012–1019.
35. Lee YH, Zhang XQ, Zhang W, Chang MT, Lin CT, Chang KD, Yu YC, Wang JT, Chang CS, Li LJ and Lin TW, Adv. Mater, 2012, 24, 2320–2325. [PubMed: 22467187]
36. Liu HF, Wong SL and Chi DZ, Chem. Vap. Deposition, 2015, 21, 241–259.
37. Lee K, Kim DH and Parsons GN, ACS Appl. Mater. Interfaces, 2014, 6, 10981–10985. [PubMed: 24979745]
38. Kim IS, Sangwan VK, Jariwala D, Wood JD, Park S, Chen KS, Shi F, Ruiz-Zepeda F, Ponce A, Jose-Yacaman M, Dravid VP, Marks TJ, Hersam MC and Lauhon LJ, ACS Nano, 2014, 8, 10551–10558. [PubMed: 25223821]
39. Jones AC and Hitchman ML, Chemical vapor deposition: Precursors, processes and applications, RSC publishing, 2009.
40. Marchand P, Hassan IA, Parkin IP and Carmalt CJ, Dalton Trans, 2013, 42, 9406–9422. [PubMed: 23629474]
41. Xu H, Zhou W, Zheng X, Huang J, Feng X, Ye L, Xu G and Lin F, Materials (Basel), 2018, 11, 870.
42. Tao L, Chen K, Chen Z, Chen W, Gui X, Chen H, Li X and Xu J-B, ACS Appl. Mater. Interfaces, 2017, 9, 12073–12081. [PubMed: 28297598]
43. Lai Z, He Q, Tran TH, Repaka DVM, Zhou D-D, Sun Y, Xi S, Li Y, Chaturvedi A, Tan C, Chen B, Nam G-H, Li B, Ling C, Zhai W, Shi Z, Hu D, Sharma V, Hu Z, Chen Y, Zhang Z, Yu Y, Renshaw Wang X, Ramanujan RV, Ma Y, Hippalgaonkar K and Zhang H, Nat. Mater, 2021, 20, 1113–1120. [PubMed: 33859384]
44. Cwik S, Mitoraj D, Mendoza Reyes O, Rogalla D, Peeters D, Kim J, Schütz HM, Bock C, Beranek R and Devi A, Adv. Mater. Interfaces, 2018, 5, 1800140.
45. Wree J-L, Ciftyurek E, Zanders D, Boysen N, Kostka A, Rogalla D, Kasischke M, Ostendorf A, Schierbaum K and Devi A, Dalton Trans, 2020, 49, 13462–13474. [PubMed: 32966456]
46. Dumcenco D, Ovchinnikov D, Lopez Sanchez O, Gillet P, Alexander DTL, Lazar S, Radenovic A and Kis A, 2D Mater, 2015, 2, 044005.
47. Imanishi N, Kanamura K and Takehara Z, J. Electrochem. Soc, 1992, 139, 2082–2087.
48. Cun H, Macha M, Kim H, Liu K, Zhao Y, LaGrange T, Kis A and Radenovic A, Nano Research, 2019, 12, 2646–2652.

49. Kranthi Kumar V, Dhar S, Choudhury TH, Shivashankar SA and Raghavan S, Nanoscale, 2015, 7, 7802–7810. [PubMed: 25849114]
50. Kang K, Xie S, Huang L, Han Y, Huang PY, Mak KF, Kim CJ, Muller D and Park J, Nature, 2015, 520, 656–660. [PubMed: 25925478]
51. McCreary KM, Cobas ED, Hanbicki AT, Rosenberger MR, Chuang H-J, Sivaram SV, Oleshko VP and Jonker BT, ACS Appl. Mater. Interfaces, 2020, 12, 9580–9588. [PubMed: 31999089]
52. Bloor LG, Carmalt CJ and Pugh D, Coord. Chem. Rev, 2011, 255, 1293–1318.
53. Marchand P and Carmalt CJ, Coord. Chem. Rev, 2013, 257, 3202–3221.
54. Malik MA, Afzaal M and O'Brien P, Chem. Rev, 2010, 110, 4417–4446. [PubMed: 20481563]
55. Ou NC, Su X, Bock DC and McElwee-White L, Coord. Chem. Rev, 2020, 421, 231459.
56. Cheon J, Gozum JE and Girolami GS, Chem. Mater, 1997, 9, 1847–1853.
57. Ouyang T, Loh KP, Zhang H, Vittal JJ, Vetrichelvan M, Chen W, Gao X and Wee ATS, J. Phys. Chem. B, 2004, 108, 17537–17545.
58. Zeng N, Hopkinson DG, Spencer BF, McAdams SG, Tedstone AA, Haigh SJ and Lewis DJ, Chem. Commun, 2019, 55, 99–102.
59. Murtaza G, Alderhami S, Alharbi YT, Zulfiqar U, Hossin M, Alanazi AM, Almanqur L, Onche EU, Venkateswaran SP and Lewis DJ, ACS Appl. Energy Mater, 2020, 3, 1952–1961. [PubMed: 32296758]
60. Lau KC, Ooi ML, Ooi ZX, Wong RCS, Choong ZL, Mazhar M and Goh BT, Electrocatalysis, 2022, 13, 182–194.
61. Brune V, Hegemann C and Mathur S, Inorg. Chem, 2019, 58, 9922–9934. [PubMed: 31310512]
62. Shupp JP, Kinne AS, Arman HD and Tonzetich ZJ, Organometallics, 2014, 33, 5238–5245.
63. Knapp CE and Carmalt CJ, Chem. Soc. Rev, 2016, 45, 1036–1064. [PubMed: 26446057]
64. Adeogun A, Afzaal M and O'Brien P, Chem. Vap. Deposition, 2006, 12, 597–599.
65. Kuddus A, Rajib A, Yokoyama K, Shida T, Ueno K and Shirai H, Nanotechnology, 2021, 33, 045601.
66. Hillenbrand J, van Gastel M, Bill E, Neese F and Fürstner A, J. Am. Chem. Soc, 2020, 142, 16392–16402. [PubMed: 32847348]
67. Dessy G, Fares V and Scaramuzza L, Acta Cryst. B, 1978, 34, 3066–3069.
68. Roberie T, Hoberman AE and Selbin J, J. Coord. Chem, 1979, 9, 79–87.
69. Roberie T, Bhacca NS, Lankin D and Selbin J, Can. J. Chem, 1980, 58, 2314–2317.
70. Grote J, Friedrich F, Berthold K, Hericks L, Neumann B, Stammler HG and Mitzel NW, Chem.-Eur. J, 2018, 24, 2626–2633. [PubMed: 29266463]
71. Dilworth JR, Richards RL, Chen GJ-J and Mcdonald JW, in Inorganic Syntheses, 1990, DOI: 10.1002/9780470132593.ch7, pp. 33–43.
72. Won YS, Kim YS, Anderson TJ, Reitfort LL, Ghiviriga I and McElwee-White L, J. Am. Chem. Soc, 2006, 128, 13781–13788. [PubMed: 17044706]
73. Won YS, Kim YS, Anderson TJ and McElwee-White L, Chem. Mater, 2008, 20, 7246–7251.
74. Li H, Wu H, Yuan S and Qian H, Sci. Rep, 2016, 6, 21171. [PubMed: 26888690]
75. Kong D, Wang H, Cha JJ, Pasta M, Koski KJ, Yao J and Cui Y, Nano Lett, 2013, 13, 1341–1347. [PubMed: 23387444]
76. Wang H, Lu Z, Xu S, Kong D, Cha JJ, Zheng G, Hsu P-C, Yan K, Bradshaw D, Prinz FB and Cui Y, Proceedings of the National Academy of Sciences, 2013, 110, 19701–19706.
77. Li Y, Majewski MB, Islam SM, Hao S, Murthy AA, DiStefano JG, Hanson ED, Xu Y, Wolverton C, Kanatzidis MG, Wasielewski MR, Chen X and Dravid VP, Nano Lett, 2018, 18, 7104–7110. [PubMed: 30296380]
78. Bhimanapati GR, Hankins T, Lei Y, Vilá RA, Fuller I, Terrones M and Robinson JA, ACS Appl. Mater. Interfaces, 2016, 8, 22190–22195. [PubMed: 27500662]
79. Li H, Zhang Q, Yap CCR, Tay BK, Edwin THT, Olivier A and Baillargeat D, Adv. Funct. Mater, 2012, 22, 1385–1390.
80. Ganta D, Sinha S and Haasch RT, Surf. Sci. Spectra, 2014, 21, 19–27.

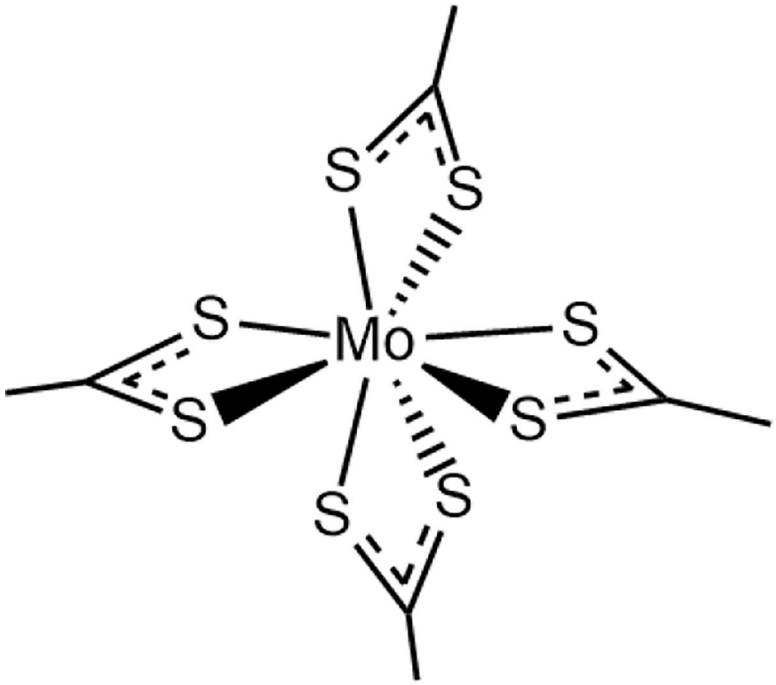

Figure 1.

The structure of $Mo(S_2CMe)_4$. The ligands are arranged in a psuedotetrahedral geometry around the molybdenum center.

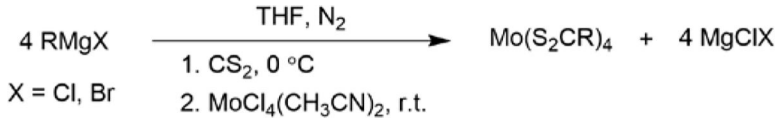

Figure 2.
Synthesis of $Mo(S_2CR)_4$.

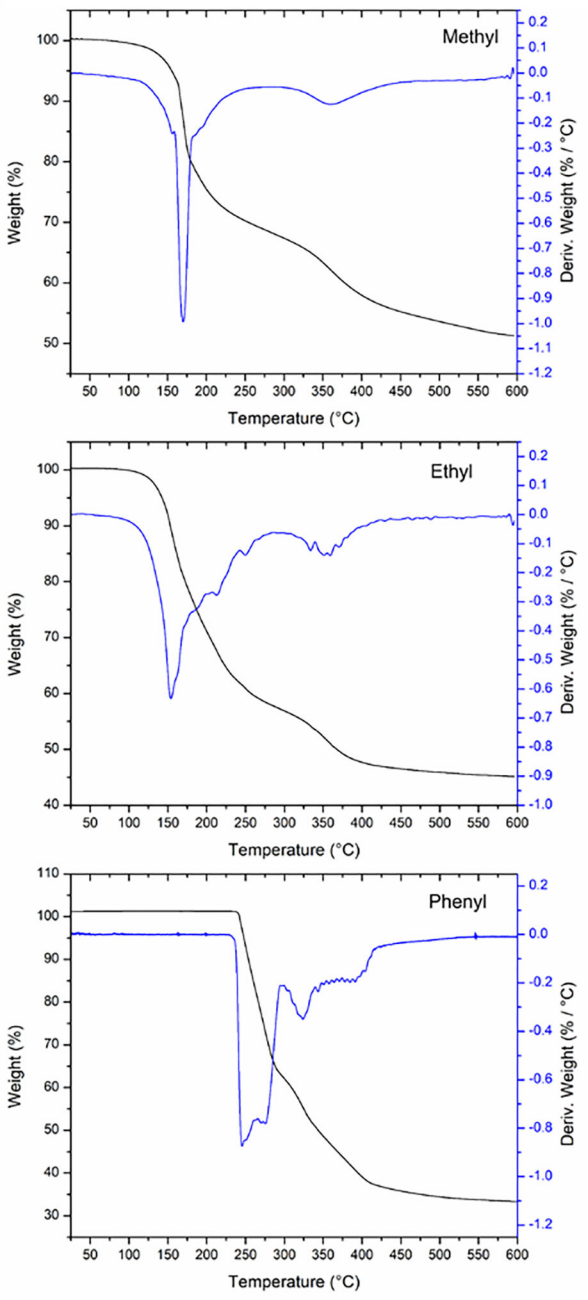

Figure 3.

TGA and first derivative curves for $Mo(S_2CMe)_4$ (top), $Mo(S_2CEt)_4$ (middle), and $Mo(S_2CPh)_4$ (bottom).

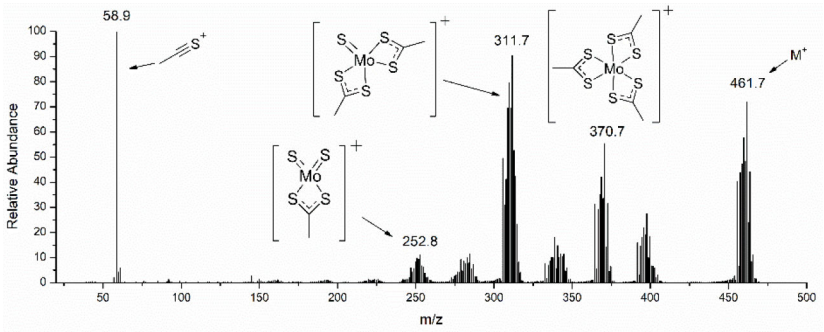

Figure 4.

DIP-EI/MS fragmentation pattern for $Mo(S_2CMe)_4$ with assigned structures of selected fragments. The relative abundances in the region from 240 to 500 m/z are enhanced by a factor of ten.

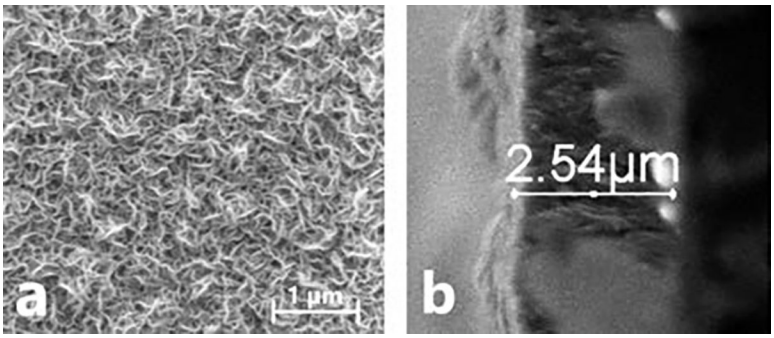

Figure 5.

a) Top-down FE-SEM image of a film grown from $Mo(S_2CMe)_4$ in toluene at 500 °C (scale bar is one micron in length), b) cross-sectional image of the same film showing a thickness of ca. 2.54 μm.

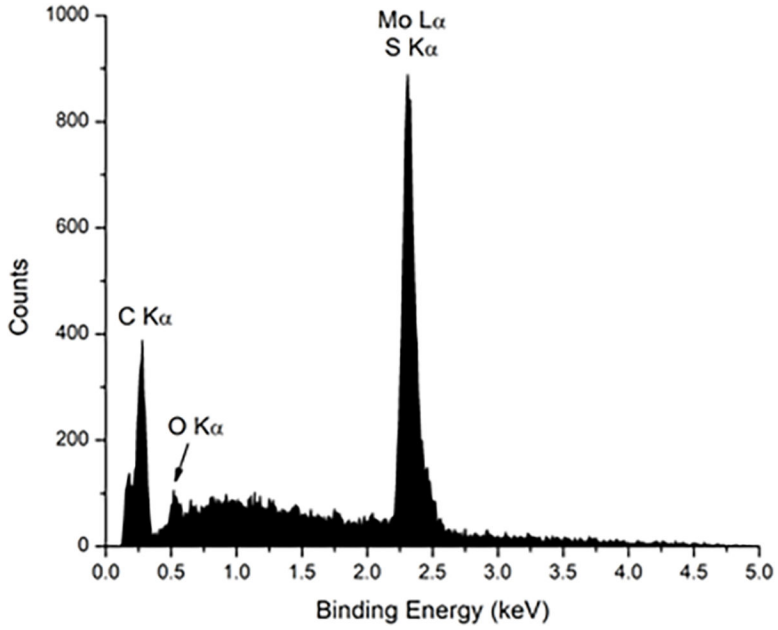

Figure 6.
EDS spectrum of a film grown from $Mo(S_2CMe)_4$ in toluene at 500 °C.

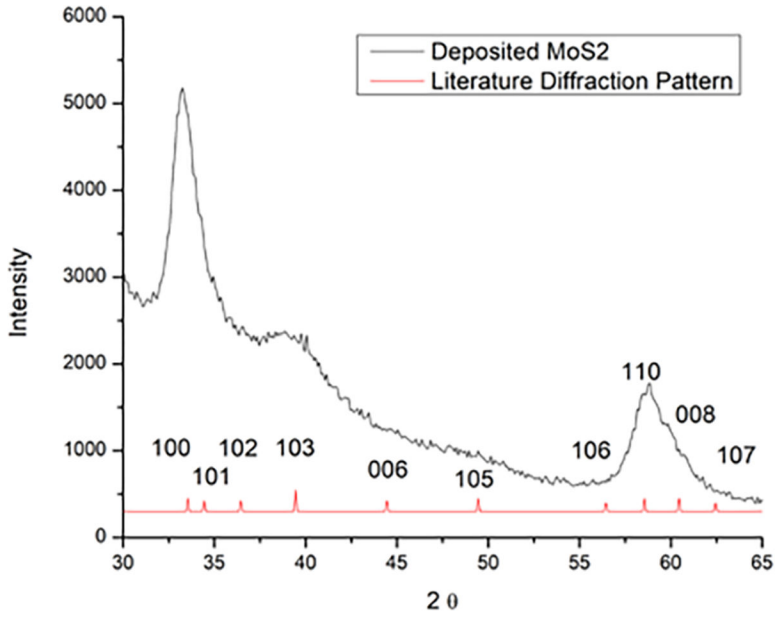

Figure 7.
GIXRD data from the film grown from $Mo(S_2CMe)_4$ at 500 °C showing the characteristic peaks of MoS_2.

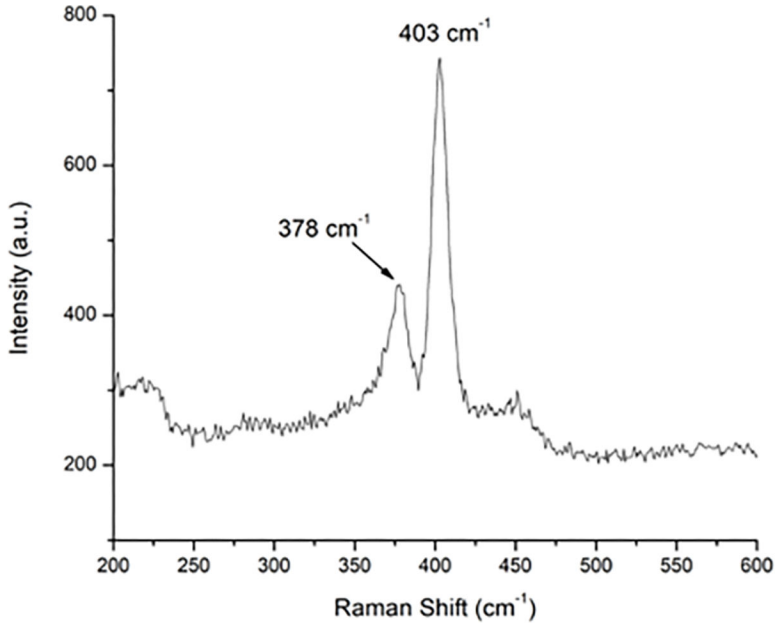

Figure 8.

Raman spectrum of a film deposited from a solution of $Mo(S_2CMe)_4$ in toluene by AACVD at 500 °C onto a silicon substrate.

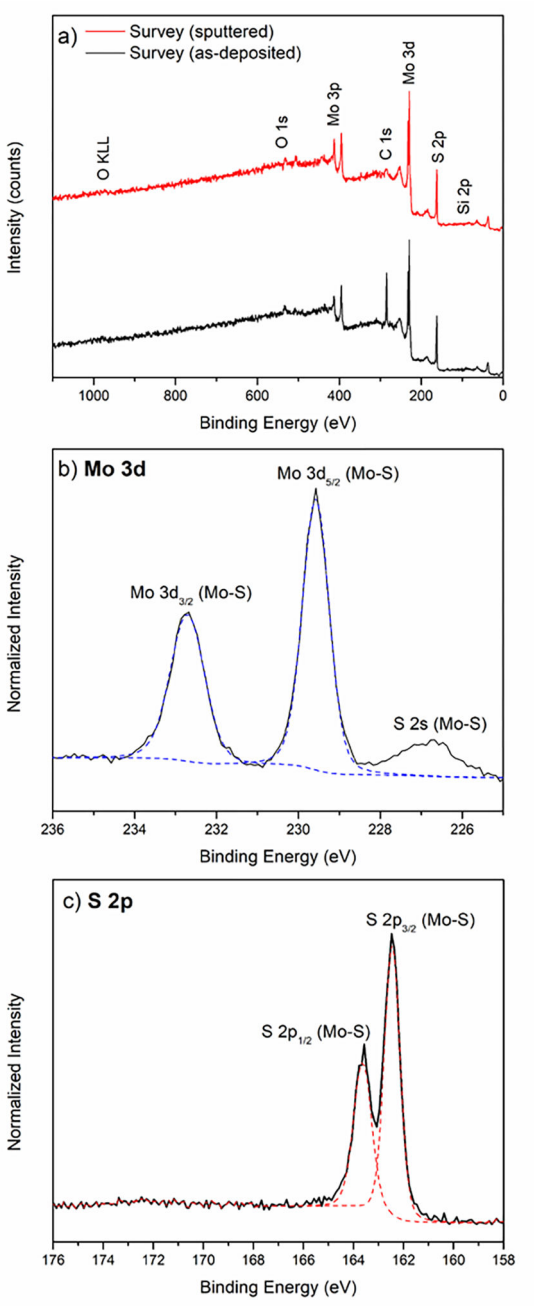

Figure 9.

a) XPS survey scan for MoS_2 grown at 500 °C. High-resolution spectra showing the (b) Mo 3d and (c) S 2p regions.

Table 1.

Selected observed ions from DIP-EI/MS of $Mo(S_2CR)_4$ complexes.

$Mo(S_2CR)_4$	$[M]^+$ m/z (%)[a]	$[SCR]^+$ m/z (%)	$[M\text{-}SCR]^+$ m/z (%.)	$[M\text{-}2(SCR)]^+$ m/z (%)	$[M\text{-}S_2CR]_3^+$ m/z (%)
$Mo(S_2CMe)_4$	461.7 (7.2)	58.9 (100)	n.o.[b]	n.o.	370.7 (5.5)
$Mo(S_2CEt)_4$	517.7 (3.2)	72.9 (100)	n.o.	n.o.	412.8 (1.0)
$Mo(S_2C^iPr)_4$	573.5 (7.4)	87.0 (100)	486.6 (1.4)	399.6 (1.1)	454.6 (1.1)
$Mo(S_2CPh)_4$	709.7 (0.4)	121.0 (100)	588.7 (0.1)	467.8 (0.1)	n.o.

[a] Relative abundances were calculated by normalizing peak intensities relative to the highest peak at 100%.

[b] n.o. = not observed.